Current Biology 21, 259–269, February 22, 2011 ©2011 Elsevier Ltd All rights reserved DOI 10.1016/j.cub.2011.01.010

Article

# PAR-4/LKB1 Mobilizes Nonmuscle Myosin through Anillin to Regulate *C. elegans* Embryonic Polarization and Cytokinesis

**Nicolas T. Chartier,[1,*] Diana P. Salazar Ospina,[1] Laura Benkemoun,[1] Mirjam Mayer,[3,4] Stephan W. Grill,[3,4] Amy S. Maddox,[1,2] and Jean-Claude Labbé[1,2]**
[1]Institute of Research in Immunology and Cancer (IRIC)
[2]Department of Pathology and Cell Biology
Université de Montréal, Montréal, H3C 3J7 Québec, Canada
[3]Max Planck Institute for the Physics of Complex Systems, 01307 Dresden, Germany
[4]Max Planck Institute for Molecular Cell Biology and Genetics, 01307 Dresden, Germany

## Summary

**Background:** The serine/threonine kinase LKB1 regulates cell growth and polarity in metazoans, and loss of LKB1 function is implicated in the development of some epithelial cancers. Despite its fundamental role, the mechanism by which LKB1 regulates polarity establishment and/or maintenance is unclear. In the present study, we use the nematode *C. elegans* to investigate the role of the LKB1 ortholog PAR-4 in actomyosin contractility, a cellular process essential for polarity establishment and cell division in the early embryo.
**Results:** Using high-resolution time-lapse imaging of GFP-tagged nonmuscle myosin II (NMY-2), we found that *par-4* mutations reduce actomyosin contractility during polarity establishment, leading to the mispositioning of anterior PAR proteins and to defects in contractile ring ingression during cytokinesis. Fluorescence recovery after photobleaching analysis revealed that the mobility of a cortical population of NMY-2 was reduced in *par-4* mutants. Interestingly, the contractility defects of *par-4* mutants depend on the reciprocal activity of ANI-1 and ANI-2, two *C. elegans* homologs of the actin cytoskeletal scaffold protein anillin.
**Conclusion:** Because loss of PAR-4 promoted inappropriate accumulation of ANI-2 at the cell cortex, we propose that PAR-4 controls *C. elegans* embryonic polarity by regulating the activity of anillin family scaffold proteins, thus enabling turnover of cortical myosin and efficient actomyosin contractility. This work provides the first description of a cellular mechanism by which PAR-4/LKB1 mediates cell polarization.

## Introduction

Cell polarization and asymmetric cell division are fundamental mechanisms required to specialize undifferentiated cells, generate cell diversity during development, and maintain tissue homeostasis in adult organisms. The *C. elegans* embryo is an outstanding model to study these processes. The *C. elegans* zygote is polarized along the anteroposterior axis so that its first division is asymmetric, resulting in two daughter cells with different sizes and fates: the larger, anterior AB cell generates most of the ectoderm, and the smaller, posterior $P_1$ cell gives rise to the endoderm and the germline [1]. Failure to properly establish anteroposterior polarity leads to misspecification of daughter cells and embryonic lethality. Polarity establishment and asymmetric cell division of the embryo are regulated by the conserved PAR proteins [2, 3]. Loss of any of the six *par* genes results in loss of polarity, subsequent abnormal symmetric cell division, and, ultimately, embryonic lethality [2].

In *C. elegans*, polarization is induced after fertilization by a sperm-derived cue that defines the future posterior pole of the embryo [4]. Soon after fertilization, the entire cortical actomyosin cytoskeleton of the embryo contracts [5], but these contractions cease near the sperm-derived pronucleus, where the actomyosin network is locally destabilized, resulting in a displacement of the contractile cortex toward the anterior pole [6]. These anterior-directed contractile flows of the actomyosin network allow the concomitant establishment of the anterior PAR-3/PAR-6/aPKC domain and the posterior PAR-2/PAR-1 domain at the cortex. The proper establishment of polarized PAR domains is ultimately crucial for asymmetric positioning of the cleavage furrow during cytokinesis. Therefore, polarization and asymmetric division of the *C. elegans* zygote rely on an intimate relationship between PAR proteins and the actomyosin cytoskeleton.

PAR-4 is a serine/threonine kinase localized symmetrically at the cortex and cytoplasm throughout polarization of the *C. elegans* embryo [7]. Mutations in *par-4* result in phenotypes shared with mutations in other *par* genes, such as compromised cytoplasmic flows during polarization, lack of germline determinant segregation, synchrony of the second embryonic divisions, and, ultimately, embryonic lethality [7, 8]. In humans, germline mutations in the *par-4* ortholog, *lkb1* (also known as *stk11*), are directly responsible for Peutz-Jeghers syndrome, a condition characterized by the development of hamartomas in the gastrointestinal tract and a predisposition to epithelial-derived cancers (reviewed in [9, 10]). Until now, two major cellular functions have been attributed to LKB1 that account for its role as a tumor suppressor: (1) regulation of energy-dependent cell growth and (2) cell polarity [11, 12]. LKB1 regulates cell growth by directly phosphorylating and activating AMP-activated protein kinase in response to energetic stress, leading to the inactivation of the mammalian target of rapamycin (mTOR) pathway [13, 14]. Although LKB1 was reported to function in polarity by remodeling the actin cytoskeleton in human epithelial cells [15, 16], its function in this process is less well understood.

To better understand the role of PAR-4 during polarization, we quantified actomyosin dynamics in early *C. elegans* embryos by high-resolution time-lapse imaging of *par-4* mutant strains transgenically expressing GFP-tagged nonmuscle myosin (NMY-2). We found that loss of PAR-4 function leads to a decrease in actomyosin contractility and to defects in segregation of anterior PAR proteins during polarity establishment. We also found that *par-4* mutations impair contractile ring ingression dynamics during the first mitotic cytokinesis and that PAR-4 activity is required for normal turnover of cortical myosin. Depletion of ANI-2, a homolog of the actomyosin scaffold protein anillin, suppresses *par-4* embryonic lethality and restores all actomyosin-dependent phenotypes observed in *par-4* mutants. We propose a model in

*Correspondence: worm.machine@gmail.com

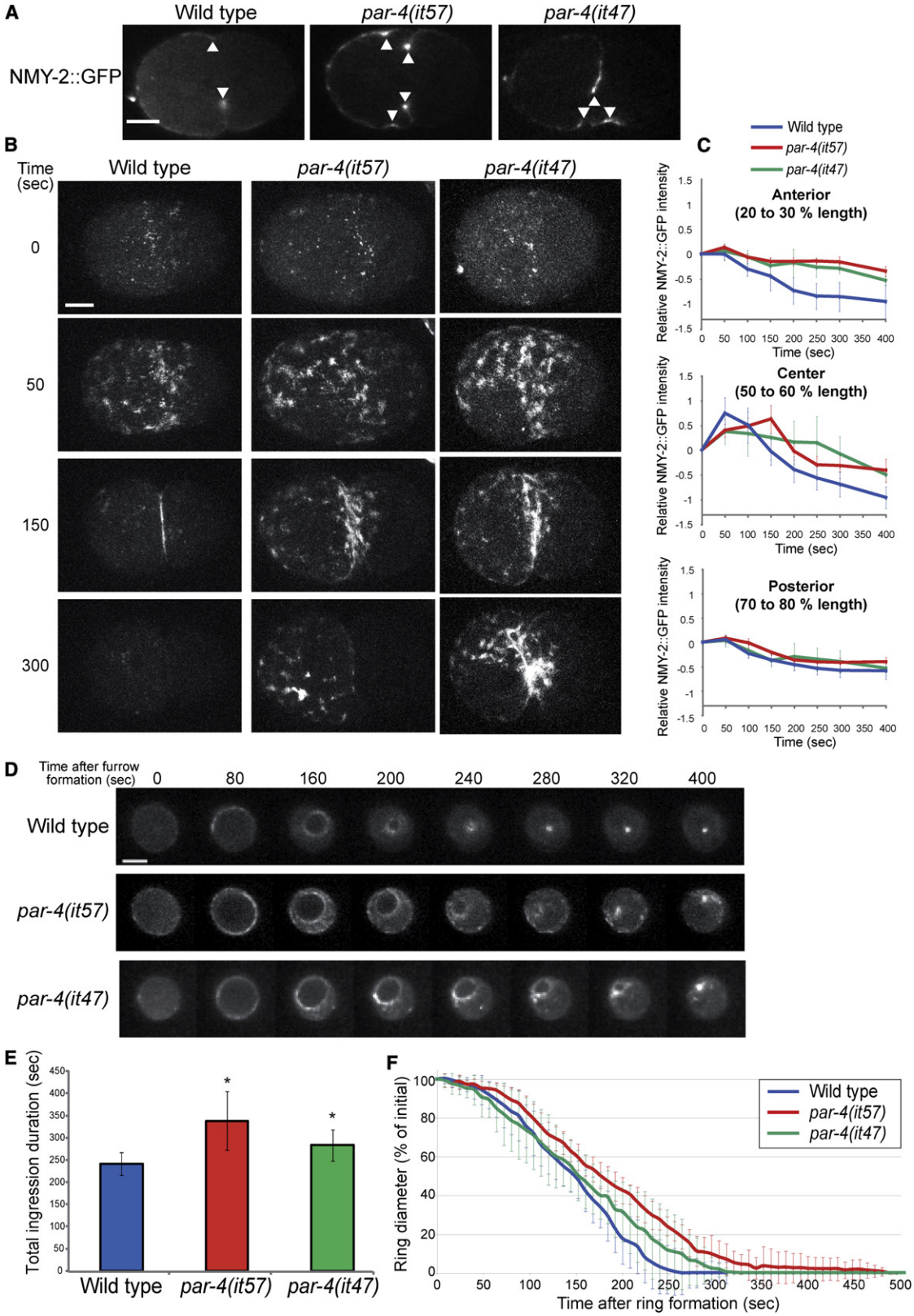


Figure 1. Mutations in *par-4* Result in Cytokinesis Defects

(A) Individual midplane images acquired during cytokinetic ring ingression of wild-type or *par-4* embryos expressing NMY-2::GFP. Images were taken from movies synchronized for each mutant background at the time of myosin recruitment at the cortex. Arrowheads point to sites of furrow ingressions and NMY-2::GFP accumulations.

(B) Sequential images showing maximal cortical NMY-2::GFP projections at different times of dividing wild-type or *par-4* embryos. Time 0 corresponds to the disappearance of anterior NMY-2::GFP fluorescence.

which PAR-4 regulates actomyosin dynamics by promoting cortical myosin mobility through anillin scaffold proteins during the early steps of *C. elegans* embryonic development.

## Results

### Cytokinetic Ring Ingression Dynamics Are Perturbed in *par-4* Mutants

In the one-cell-stage *C. elegans* embryo, mutations in *par-4* result in a unique phenotype during the first cytokinesis: the membrane adjacent to the contractile ring forms protrusions previously referred to as blebs [8]. We hypothesized that these cortical protrusions in *par-4* embryos reflect misregulation of the dynamics of actomyosin contractility, a process that has to be tightly controlled and accurately localized during cytokinesis. To analyze the dynamics of the actomyosin cytoskeleton, we used two strains mutant for distinct thermosensitive alleles of *par-4* (*it47* and *it57*) expressing NMY-2::GFP and imaged the first mitotic division by time-lapse microscopy. We observed multiple, disorganized ingressions that indicated lateral instability of the division plane (Figure 1A; see also Movie S1 available online). Such abnormal furrowing during cytokinesis can be due to defects in the assembly of the contractile ring. To test this possibility, we analyzed the cortical recruitment of NMY-2::GFP in wild-type and *par-4* embryos during cytokinesis. Around the time of anaphase onset, the anterior cortical domain of actomyosin was dispersed, and NMY-2::GFP rapidly accumulated in cortical patches at the future site of cleavage to form the contractile ring (Figure 1B and Movie S1). In *par-4* mutant embryos, formation of cortical patches started at the same time as in wild-type, but their coalescence into the cytokinetic furrow was delayed. Analysis of mean cortical fluorescence intensity revealed that NMY-2::GFP was recruited to a larger region of the cortex in *par-4* embryos (Figure 1B and Figure S1) and that the anterior cortex remained enriched in NMY-2::GFP patches longer than wild-type embryos (Figure 1C and Figure S1). Whereas NMY-2::GFP patches coalesced into the cytokinetic furrow by 150 s after anterior domain dispersion in wild-type controls, they were still present at the cortex of *par-4* mutants even after 300 s (Figure 1B and Figure S1). We conclude that specification of the cleavage furrow is compromised in *par-4* mutant embryos and is associated with a longer contractile phase during cytokinesis.

To test whether perturbations of the contractile ring could induce changes in the dynamics of ring closure, we mounted embryos vertically and imaged cytokinetic furrow ingression by time-lapse microscopy (Figure 1D and Movie S2). We found that the total time from furrow formation to complete closure was increased by 15%–30% in *par-4* mutants compared to wild-type embryos (Figure 1E). This indicates that PAR-4 is required for the proper kinetics of cytokinetic furrow ingression. Interestingly, the initiation of ingression was similar between wild-type and *par-4* mutant embryos during the first minute following ring formation, but, whereas it accelerated in wild-type controls after 100 s, the rate of closure remained constant or started decreasing in *par-4* mutants (Figure 1F and Figure S1B). Together, these results indicate that PAR-4 regulates cytokinesis by ensuring proper furrow specification and promoting the rate of contractile ring ingression; these results are consistent with the hypothesis that PAR-4 affects the cortical dynamics of the actomyosin network.

### Mutations in *par-4* Reduce Actomyosin Contractility during Polarity Establishment

Like cytokinesis, polarization of the early *C. elegans* embryo also depends on actomyosin contractility. Polarization occurs via an anterior-directed contractile flow of the cortical actomyosin network that initiates after the completion of maternal meiosis, allowing the proper segregation of anterior and posterior PAR domains [6]. Because *par-4* embryos exhibit polarity defects, we investigated whether cortical actomyosin dynamics are perturbed during the polarization phase by imaging the cortex of newly fertilized wild-type and *par-4* embryos using time-lapse microscopy (Movie S3). Quantitative kymograph analysis showed that NMY-2::GFP foci moved 30% more slowly toward the anterior in *par-4* mutant embryos compared to wild-type controls (Figures 2A and 2B). Contractility dynamics were specifically affected, because we did not observe any obvious modification in the organization of the myosin network: the number and the area of NMY-2::GFP foci in *par-4* mutants were identical to wild-type embryos during the polarization phase (Figures S1C and S1D). These results indicate that *par-4* is required for efficient contraction during polarization of the early embryo.

At the end of the polarization phase, cortical contractions cease and NMY-2::GFP is enriched at the anterior half of the embryo. Because a reduction in the velocity of NMY-2::GFP could affect the size of this anterior domain, we compared the position of cortical NMY-2::GFP domain in wild-type and *par-4* mutants by measuring the fluorescence intensity around the entire perimeter of the embryo after polarization (Figures 2C–2F). We observed that the domain of detectable cortical NMY-2::GFP extended farther toward the posterior in *par-4* embryos than in wild-type (Figure 2D, right panels). The mean length of cortex where fluorescence intensity was within 70% of the maximal NMY-2::GFP signal was significantly larger in *par-4* mutants than in wild-type controls (Figure 2F). Similar results were obtained when measurements were made with a threshold of 50% of the maximal intensity (data not shown). This indicates that the reduction of contraction velocity reduced the total displacement of cortical NMY-2::GFP toward the anterior pole in embryos lacking PAR-4 function.

The anterior localization of cortical PAR-6 protein during polarization depends on actomyosin contractility [6] and thus should also depend on PAR-4. We tested whether the localization of PAR-6 was affected by *par-4* mutations in embryos

(C) Quantification of the relative fluorescence intensity ± standard error of the mean (SEM) of cortical NMY-2::GFP along the anteroposterior axis in wild-type (blue line, n = 5), *par-4(it57)* (red line, n = 4), and *par-4(it47)* (green line, n = 3) embryos.

(D) Sequential images showing the ingression of the cytokinetic ring at different times in vertically mounted wild-type or *par-4* embryos expressing NMY-2::GFP. For each strain, time 0 corresponds to the first frame showing cortical recruitment of NMY-2::GFP.

(E) Quantification of the mean duration of cytokinetic furrow ingression ± standard deviation (SD) (from furrow formation to enclosure) in wild-type (241.3 ± 25.5 s, n = 6), *par-4(it57)* (338.0 ± 65.8 s, n = 8), and *par-4(it47)* (283.2 ± 35.1 s, n = 5) embryos. *$p < 0.05$ (Student's t test).

(F) Quantification of the kinetics of contractile ring closure ± SD in wild-type (blue line, n = 6), *par-4(it57)* (red line, n = 8), and *par-4(it47)* (green line, n = 5). The furrow diameter at each time point is compared to the initial diameter. In all panels, anterior is to the left (except in D) and scale bar is 10 μm. See also Figure S1, Movie S1, and Movie S2.

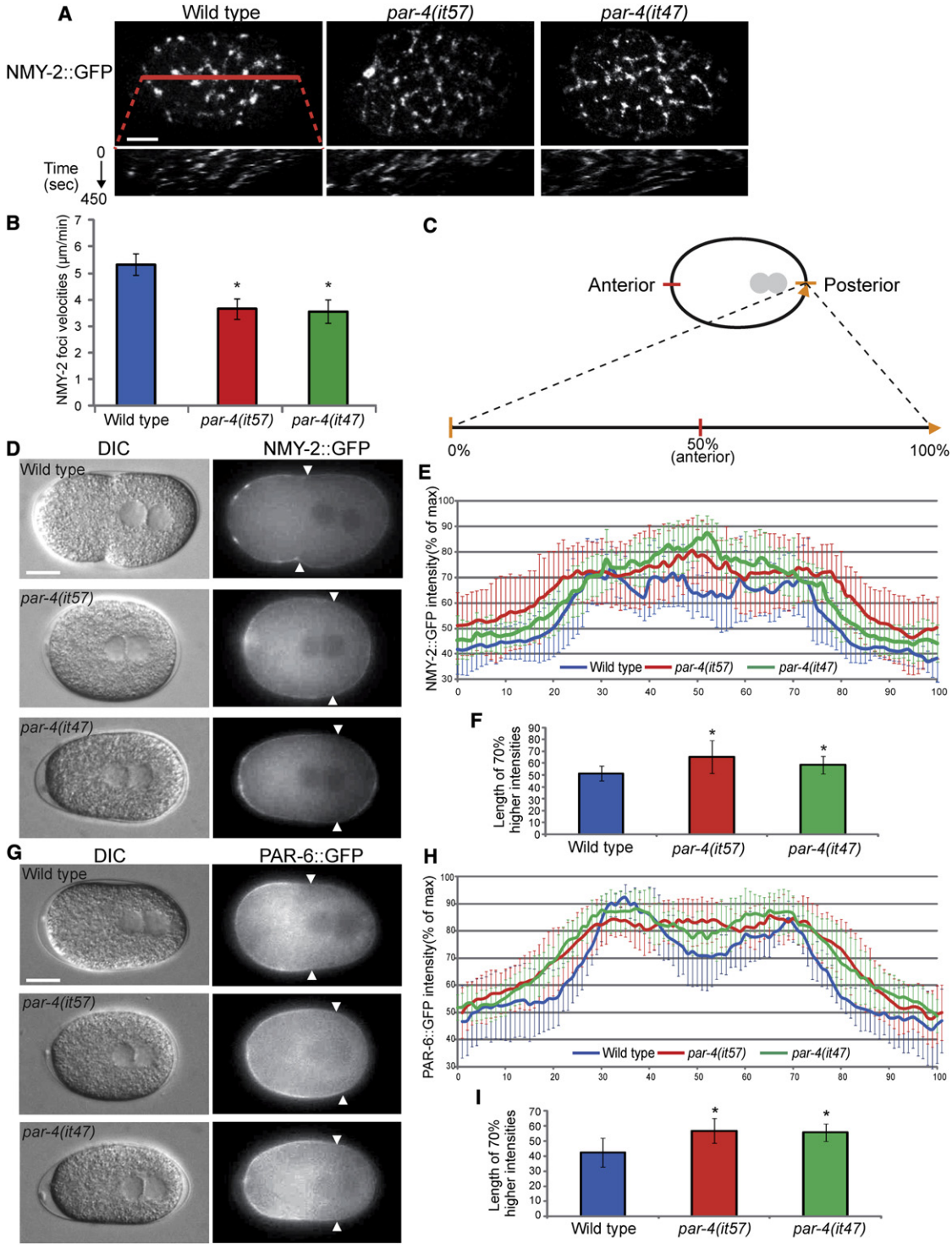


Figure 2. Polarity Establishment Is Compromised in *par-4* Embryos

(A) Cortical NMY-2 foci were imaged by time-lapse microscopy in wild-type or *par-4* mutant embryos. Bottom panels show representative kymographs created along the anteroposterior axis from the beginning of anterior movements.

(B) Quantification of the velocities ± SD of NMY-2::GFP foci calculated from kymographs at the posterior of wild-type (5.3 ± 1.2 μm/min, n = 7), *par-4(it57)* (3.7 ± 0.7 μm/min, n = 8), and *par-4(it47)* (3.8 ± 0.6 μm/min, n = 9) embryos. Twelve individual foci were quantified per embryo.

(C) Schematic representation of the method used to quantify cortical domains presented in Figures 1D–1I.

(D) Differential interference contrast (DIC) and epifluorescence images showing the extent of NMY-2 cortical domain in wild-type, *par-4(it57)*, and *par-4(it47)* embryos at the time of pronuclei meeting. Arrowheads indicate the estimated limit of NMY-2 domains for each condition.

(E) Quantification ± SD of the distribution of NMY-2::GFP compared to the maximal intensity of NMY-2::GFP around the cortex in wild-type (blue line, n = 10), *par-4(it57)* (red line, n = 9), and *par-4(it47)* (green line, n = 9) embryos. The 50% mark is at the anterior pole.

(F) Quantification of the mean percentage ± SD of cortical perimeter occupied by 70% of the maximal NMY-2::GFP intensity.

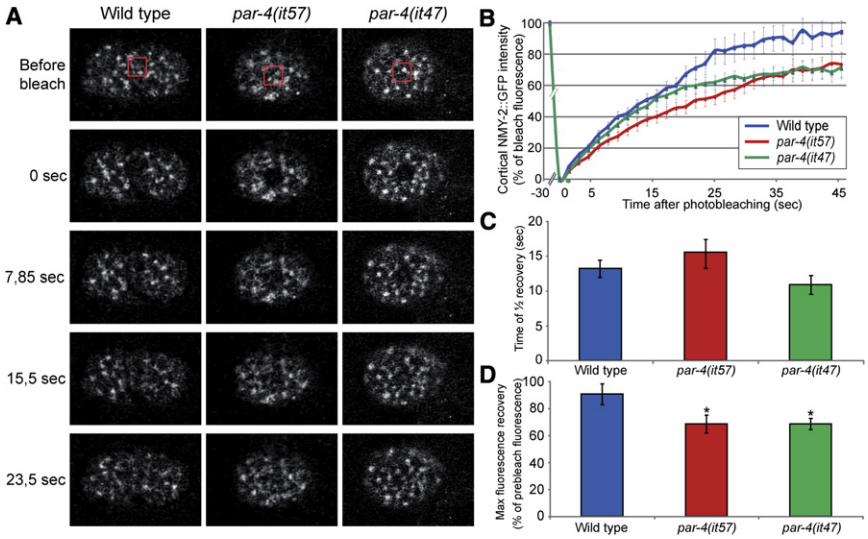


Figure 3. A Nonmobile NMY-2::GFP Fraction Increases in *par-4* Embryos

(A) Sequential confocal images of cortical NMY-2::GFP before and after photobleaching a 20 × 20 pixel region (red square) in wild-type and *par-4* embryos treated with *spd-5(RNAi)*. Time 0 corresponds to the first frame following photobleaching. Scale bar is 10 μm.

(B) Quantification of FRAP ± SEM in wild-type (blue line, n = 13), *par-4(it57)* (red line, n = 13), and *par-4(it47)* (green line, n = 12) embryos.

(C) Quantification of the time of half fluorescence recovery ± SEM in wild-type (13.2 ± 1.3 s), *par-4 (it57)* (15.5 ± 2.2 s), and *par-4(it47)* (10.9 ± 1.4 s).

(D) Quantification of the percentage of maximal fluorescence recovery ± SEM in wild-type (90.7% ± 7.7%), *par-4(it57)* (68.6% ± 6.6%), and *par-4(it47)* (68.6% ± 4.2%). *p < 0.05 (Student's t test). See also Figure S2.

transgenically expressing PAR-6::GFP (Figures 2G–2I). As expected for a condition in which contractility is defective, distribution of cortical PAR-6::GFP extended farther into the posterior in *par-4* mutants than in wild-type controls (Figures 2H and 2I). Overall, these results demonstrate that PAR-4 is required for proper specification of the anterior PAR protein cortical domain through its role in regulating actomyosin contractility.

### PAR-4 Is Specifically Required to Mobilize a Population of NMY-2 at the Cortex

Our observations that NMY-2::GFP dynamics are reduced in *par-4* mutant embryos indicate that loss of PAR-4 function compromises actomyosin contractility. These defects could result from a reduction in myosin contractile efficiency (i.e., a catalytic defect) or from a defect in myosin turnover (i.e., a structural defect) during contractility.

To test whether the activity of myosin II was reduced in *par-4* mutants, we analyzed the cortical tension of the actomyosin network by performing laser-cutting experiments on the actomyosin cytoskeleton during the polarization phase in wild-type and *par-4* embryos (Figure S2). Laser cutting induces a cytoskeletal recoil, and differences in tension within the cytoskeleton are observed as differences in the recoil velocity of cortex adjacent to the cut site [17]. If contractile tension is affected by *par-4* mutations, the recoil velocity would be reduced in *par-4* embryos compared to wild-type controls. However, no difference was observed when measuring tension in the direction orthogonal to flow (Figure S2), indicating that the myosin II-dependent contractile tension applied to the cytoskeleton, and thus myosin II activity, is normal in *par-4* mutants.

Changes in structural regulation of the cortical cytoskeleton can be assayed by measuring molecular turnover. A decrease in myosin turnover was shown to affect the viscoelastic properties of the actomyosin cortex during polarization [17] and could therefore result in a reduction of cortical flow velocity. To determine whether PAR-4 regulates molecular dynamics of cortical cytoskeleton, we measured NMY-2::GFP turnover during the polarization phase by fluorescence recovery after photobleaching (FRAP) (Figure 3). Experiments were performed using embryos depleted of the protein SPD-5 to eliminate the confounding effects of mass anteriorward movements of NMY-2::GFP [6, 17]. NMY-2::GFP was photobleached in wild-type and *par-4* mutant embryos, and FRAP was monitored by confocal microscopy (Figure 3A). No significant difference was observed in the time of half-recovery of NMY-2::GFP fluorescence between wild-type and *par-4* mutants (Figures 3B and 3C). In contrast, the maximal recovery of fluorescence was reduced by 20% in *par-4* embryos (Figures 3B and 3D). The maximal recovery of fluorescence represents the mobile fraction of NMY-2::GFP, whereas the percentage of fluorescence that does not recover comprises the nonmobile fraction. A reduction in maximal fluorescence recovery indicates an increase in a nonmobile fraction of NMY-2::GFP in *par-4* mutants compared to wild-type. Thus, PAR-4 functions during embryonic polarization to mobilize a population of nonmuscle myosin II at the cortex to promote proper actomyosin dynamics.

### Disruption of *ani-2* Suppresses *par-4* Embryonic Lethality

Actomyosin dynamics are mediated by a complex coordination involving many proteins. Central to this regulation are scaffolding proteins, such as anillin, which can bind to multiple cortical regulators simultaneously [18]. Interestingly, an RNA interference (RNAi)-based screen for suppressors of *par-4* lethality (N.T.C., D.P.S.O., and J.-C.L., unpublished data) identified the gene *ani-2*, which encodes one of the three *C. elegans* homologs of anillin [19]. Depletion of ANI-2 by feeding RNAi suppressed the lethality of both thermosensitive alleles of *par-4* at the semipermissive temperatures of 18°C and 20°C, but not at the fully restrictive temperature of 25°C

(G) Same as in (D), but for PAR-6.

(H) Quantification ± SD of the distribution of PAR-6::GFP compared to the maximal intensity of PAR-6::GFP around the cortex in wild-type (blue line, n = 9), *par-4(it57)* (red line, n = 12), and *par-4(it47)* (green line, n = 11) embryos.

(I) Quantification of the mean percentage ± SD of cortical perimeter occupied by 70% of the maximal PAR-6::GFP intensity. In all panels, anterior is to the left, scale bar is 10 μm, and *p < 0.05 (Student's t test). See also Figure S1 and Movie S3.

Table 1. Depletion of *ani-2* Suppresses *par-4* Lethality

| Temperature | Genotype | Hatching Progeny (%) after RNAi | | | |
|---|---|---|---|---|---|
| | | Control | *ani-2* | *ani-1* | *ani-3* |
| 25°C | Wild-type | 98.4 ± 1.6 | 91.1 ± 3.9 | 55.2 ± 6.6 | 97.5 ± 1.6 |
| | *par-4(it57)* | 0 | 0 | 0 | 0 |
| | *par-4(it47)* | 0 | 0 | 0 | 0 |
| | *ani-2(ok1147/+);par-4(it57)* | 0 | 0 | 0 | 0 |
| 20°C | Wild-type | 99.7 ± 0.3 | 93.0 ± 3.3 | 70.3 ± 9.9 | 99.4 ± 0.3 |
| | *par-4(it57)* | 0 | 1.4 ± 0.2[a] | 0 | 0 |
| | *par-4(it47)* | 1.0 ± 0.2 | 8.2 ± 1.1[a] | 0 | 1.4 ± 1.1 |
| | *ani-2(ok1147/+);par-4(it57)* | 0.1 ± 0.1 | 1.0 ± 0.5 | 0 | 0 |
| 18°C | Wild-type | 99.4 ± 0.6 | 98.6 ± 0.7 | 55.5 ± 6.7 | 99.1 ± 0.2 |
| | *par-4(it57)* | 9.9 ± 3.4 | 33.0 ± 2.4[a] | 4.6 ± 1.8 | 19.0 ± 3.8 |
| | *par-4(it47)* | 8.0 ± 2.1 | 26.7 ± 1.3[a] | 3.3 ± 1.1 | 15.2 ± 2.7 |
| | *ani-2(ok1147/+);par-4(it57)* | 25.8 ± 5.8[a,b] | 51.8 ± 12.0[a,b] | 3.4 ± 0.6 | 20.6 ± 3.8 |
| 22°C | *par-1(zu310)* | 37.8 ± 8.4 | 32.7 ± 11.7 | ND | ND |

The value corresponds to embryonic viability, i.e., the average percentage of embryos that hatched over the total number of embryos (n > 1000 for each condition) ± standard error of the mean over three independent assays. ND denotes not determined.
[a] The value is significantly different ($p < 0.01$, Student's t test) from the same strain treated with control*(RNAi)*.
[b] The value is significantly different ($p < 0.05$, Student's t test) from *par-4* mutants treated with control*(RNAi)*.

(Table 1), suggesting that it regulates a single, discrete, PAR-4-dependent pathway that is essential only when PAR-4 activity is mildly compromised. Depletion of the other two anillin isoforms in *C. elegans* (ANI-1 and ANI-3) did not suppress *par-4* lethality, indicating that this phenotype specifically depends on ANI-2 depletion. To confirm specificity, we analyzed whether deletion of *ani-2* can suppress *par-4* lethality. Because homozygous deletion of *ani-2* leads to sterility, thus precluding the quantification of embryonic viability, we performed experiments in a strain heterozygous for *ani-2* deletion. We found that reducing *ani-2* gene dosage by half significantly increased the number of viable *par-4* mutant embryos at 18°C, and depleting *par-4(it57ts); ani-2(+/−)* animals of ANI-2 by RNAi further increased embryonic viability (Table 1). These results demonstrate that the suppression of embryonic lethality resulting from loss of *par-4* function by *ani-2* is specific. Furthermore, dose-dependent suppression by loss of ANI-2 suggests a structural as opposed to catalytic mechanism.

PAR-4/LKB1 has been proposed to function upstream of the PAR-1 kinase [20, 21]. We therefore tested whether *ani-2 (RNAi)* could also restore the viability of a thermosensitive allele of *par-1(zu310)* and found that it had no effect on the viability of *par-1* embryos at the semipermissive temperature of 22°C (Table 1). This indicates that ANI-2 antagonizes PAR-4 activity independently of PAR-1 and is consistent with PAR-1 being dispensable for cortical flows [22].

## PAR-4 Modulates the Localization of ANI-2 in Early Embryos

The suppression of *par-4* early embryonic lethality by *ani-2* depletion indicates that the two proteins act antagonistically, perhaps in a common pathway. To test whether *ani-2* functions upstream of PAR-4, we assessed the levels of PAR-4 protein by western blot analysis in embryonic extracts of animals treated with control or *ani-2(RNAi)* and found that they were normal (Figure S3). Furthermore, we observed that PAR-4 localization was normal following ANI-2 depletion (Figure 4B). Thus, ANI-2 is not required for proper PAR-4 protein levels or localization in early embryos.

An alternate hypothesis is that PAR-4 acts upstream of ANI-2. To assess this, we examined ANI-2 localization in fixed wild-type and *par-4* embryos (Figure 4A). As previously reported [19], ANI-2 does not localize to the membrane of wild-type embryos, but rather to puncta throughout the cytoplasm. These puncta were not detected in embryos depleted of ANI-2 by RNAi, demonstrating the specificity of this pattern (Figure 4B). Interestingly, *par-4* mutant embryos had an increased number of cytoplasmic ANI-2 puncta (Figure S3C) and displayed cortical accumulations of ANI-2, mainly at the membrane between the two blastomeres (Figure 4C). Cortical ANI-2 was detectable in less than 10% of wild-type embryos but in 85% of *par-4* mutant embryos. We also observed that ANI-2 accumulated in the midbodies formed following abnormal cytokinetic furrows in *par-4* mutants (Figure 4D and Figure S3D). These results indicate that ANI-2 localizes to the cortex when PAR-4 activity is compromised and suggest that PAR-4 acts upstream of ANI-2, regulating actomyosin contractility by preventing ectopic accumulation of ANI-2 at the cortex.

## Depletion of ANI-2 Partially Suppresses All Actomyosin-Dependent Phenotypes of *par-4*

Anillin is a scaffold protein important for the organization of actomyosin contractility regulators (reviewed in [18]). Our findings that *ani-2* suppresses *par-4* lethality and that *par-4* mutants have actomyosin contractility defects suggested the possibility that these defects are due to ectopically active ANI-2. We therefore tested whether depleting ANI-2 by RNAi significantly suppressed the actomyosin contractility defects displayed by *par-4* mutants at fully restrictive temperature. In these conditions, we measured a restoration of the velocity of NMY-2::GFP foci during polarization (Figures 5A and 5B), the position of NMY-2::GFP and PAR-6::GFP at the end of polarization (Figures 5C–5E and Figure S4), persistence of NMY-2 cortical patches in the anterior during cytokinesis (Figure S4), and the kinetics of contractile ring closure (Figures 5F and 5G). Finally, depleting ANI-2 increased myosin turnover in *par-4* embryos (Figures 5H and 5I). ANI-2 depletion did not lead to a significant modification of these phenotypes in wild-type embryos, indicating that ANI-2 activity is higher in *par-4* mutants compared to wild-type animals. These results indicate that all of the actomyosin-dependent defects observed in *par-4* mutant embryos are caused by a gain of ANI-2 function.

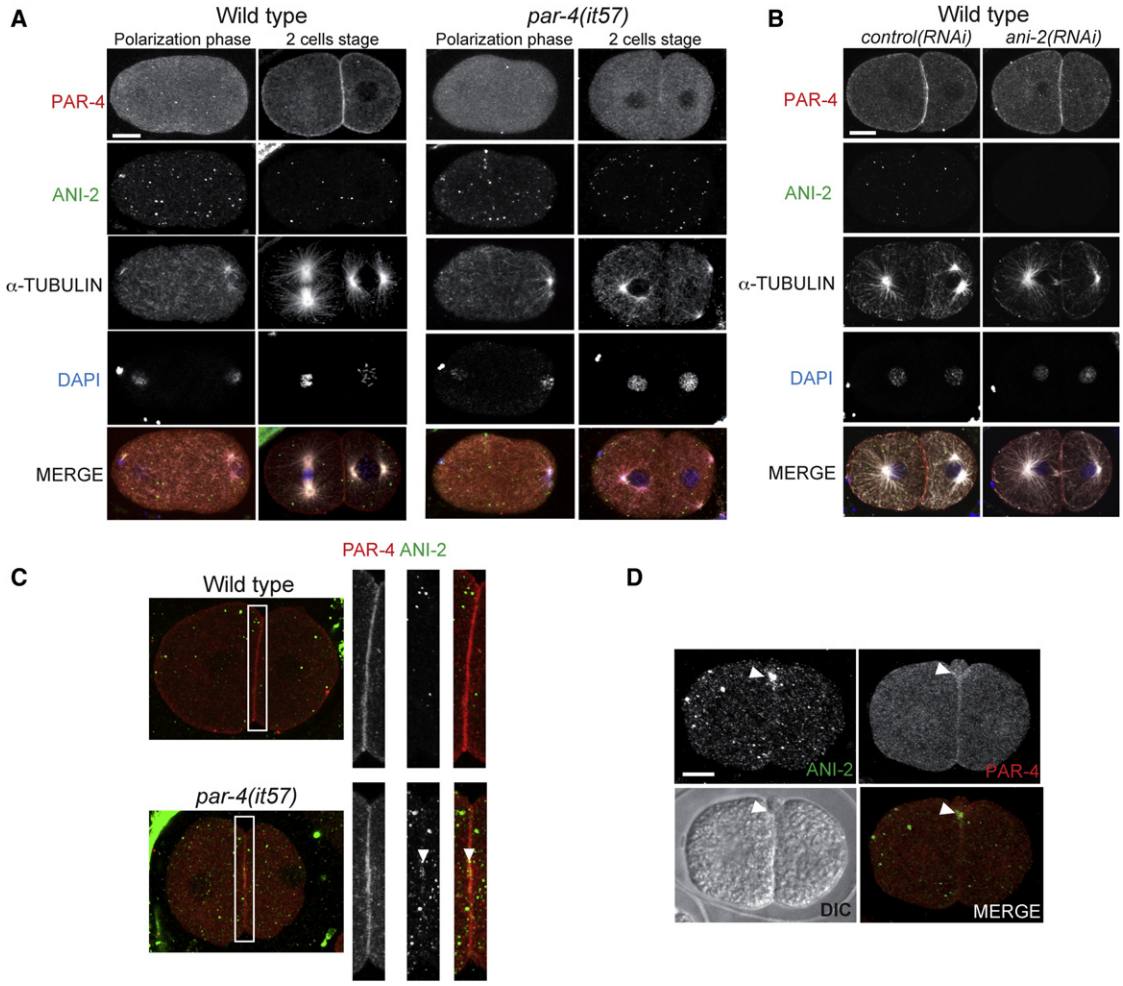


Figure 4. PAR-4 Modulates ANI-2 Localization in Early Embryos

(A) Maximal-projection images of ten confocal midplane sections (of 1 μm each) of wild-type or *par-4(it57)* embryos immunostained with antibodies against the indicated proteins, at the time of polarization and at the two-cell stage.

(B) Same as in (A) for control or *ani-2(RNAi)* wild-type embryos immunostained with antibodies against the indicated proteins.

(C) Wild-type or *par-4(it57)* embryos immunostained with antibodies against PAR-4 and ANI-2. Insets are magnified (2×) to show cortical accumulation (arrowhead) of ANI-2 in *par-4* embryos (see quantification in Figure S3).

(D) Same as in (A) for a *par-4(it47)* two-cell stage embryo with a site of multiple furrow ingression (arrowhead) and immunostained with antibodies against PAR-4 and ANI-2. In all panels, anterior is to the left and scale bar is 10 μm. See also Figure S3.

Embryos lacking PAR-4 function display several phenotypes that do not only depend on actomyosin contractility, such as defective segregation of cell fate determinants (PIE-1 protein, P granules) and reduced asynchrony between the divisions of AB and $P_1$ blastomeres [2, 8]. Disruption of *ani-2* did not suppress these phenotypes (Figure S5), indicating that the role of ANI-2 is specific to actomyosin contractility and that ANI-2 functions independently of other PAR-4-dependent pathways that contribute to overall embryo polarization and viability (see Discussion).

## PAR-4 Regulates the Balance between ANI-1 and ANI-2 Functions

The N-terminal part of *Drosophila* or human anillin contains formin-, myosin-, and actin-binding domains; the C-terminal part contains an anillin homology domain (AHD), which interacts with actin regulator RhoA and the small GTPase regulator MgcRacGAP, and a PH domain that can interact with septins [23–26]. In *C. elegans*, the canonical anillin protein ANI-1 is predicted to have all four domains; it organizes cortical contractility during polarization and the asymmetric closure of the cytokinetic furrow [19, 27]. ANI-2 is a shorter isoform of anillin that lacks the N-terminal domains predicted to bind myosin and actin [19]. By competing with ANI-1 for the binding of C-terminal domain partners, this shorter isoform could function in a dominant-negative manner and thus negatively regulate actomyosin contractility. To test this, we depleted ANI-1 from wild-type and *par-4* embryos and measured the kinetics of contractile ring closure, as well as the position of PAR-6::GFP domain at the end of polarization. We found that although ANI-1 depletion had no effect on the position of cortical PAR-6::GFP, it caused an increase in the duration of cytokinetic ring ingression in *par-4* mutant embryos (Figure 6A). This is consistent with previous work showing that ANI-1 is dispensable for proper polarization, whereas it is required for asymmetric ingression during cytokinesis [19, 27]. Importantly, simultaneous depletion of ANI-2 and ANI-1 failed to suppress both phenotypic defects displayed by *par-4*

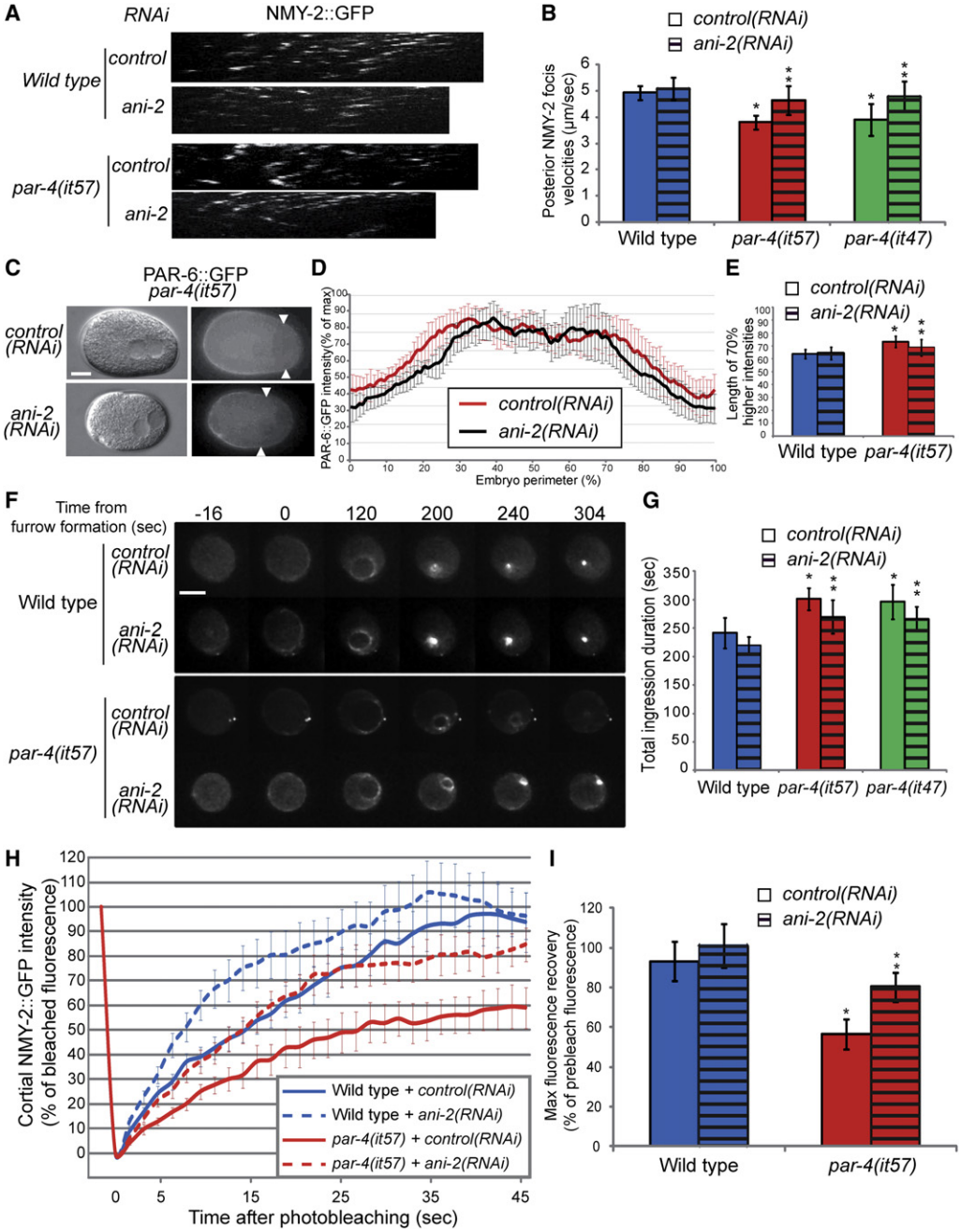


Figure 5. Disruption of *ani-2* Partially Suppresses All Actomyosin-Dependent Phenotypes of *par-4* Embryos

(A) Representative kymographs showing the polarized movements of NMY-2::GFP along the anteroposterior axis in wild-type and *par-4* mutant embryos treated for 24 hr with control (vector alone) or *ani-2(RNAi)*. Anterior is to the left.

(B) Quantification of the velocities of NMY-2::GFP foci ± SD at the posterior of wild-type and *par-4* embryos treated for 24 hr with control (solid bars) or *ani-2 (RNAi)* (striped bars); n = 10–13 for each condition.

(C) DIC (left panels) and epifluorescence (right panels) images showing the extent of PAR-6 cortical domain at the time of pronuclei meeting in *par-4(it57)* embryos treated with control or *ani-2(RNAi)*. Arrowheads indicate the estimated limit of PAR-6 domains for each condition. Anterior is to the left.

(D) Quantification ± SD of the distribution of PAR-6::GFP compared to the maximal intensity of PAR-6::GFP around the cortex in control (red line, n = 9) or *ani-2(RNAi)* (black line, n = 9) embryos.

(E) Quantification of the mean percentage ± SD of cortical perimeter occupied by 70% of the maximal PAR-6::GFP intensity in strains treated with control (solid bars) or *ani-2(RNAi)* (striped bars).

(F) Sequential images showing the ingression of the cytokinetic ring at different times in vertically mounted wild-type or *par-4* embryos expressing NMY-2::GFP and treated with control or *ani-2(RNAi)*. For each strain, time 0 corresponds to the first frame showing cortical recruitment of NMY-2::GFP.

(G) Quantification of the mean duration of cytokinetic furrow ingression ± SD (from furrow formation to enclosure) in each strain treated with control (solid bars) or *ani-2(RNAi)* (striped bars); n = 8–12 for each condition.

(H) Quantification of FRAP ± SEM in wild-type (red lines) and *par-4(it57)* (blue lines) embryos treated with control (solid lines) or *ani-2(RNAi)* (dashed lines); n = 9–13 for each condition.

**A**

| Genotype | *RNAi* treatment | Duration of ingression (sec) | Distribution of PAR-6::GFP intensities at pronuclei meeting (% of embryo length) | Maximal NMY-2::GFP fluorescence recovery after FRAP |
|---|---|---|---|---|
| *Wild-type* | *control* | 242 ± 27 (11) | 63.71 ± 4.56 (14) | 93.26 ± 10.04 (13) |
| | *ani-2* | 220 ± 15 (8) | 64.33 ± 7.96 (15) | 101.34 ± 10.92 (12) |
| | *ani-1+ control* | 270 ± 34 (5) | 60.33 ± 5.72 (6) | 88.27 ± 6.55 (9) |
| | *ani-1 + ani-2* | 226 ± 15 (5) | 62.38 ± 9.30 (8) | ND |
| *par-4* | *control* | 296 ± 30 (10) | 73.22 ± 4.84 (9) | 56.42 ± 7.67 (9) |
| | *ani-2* | 266 ± 21 * (8) | 68.67 ± 3.71 * (9) | 80.37 ± 7.18 * (11) |
| | *ani-1+ control* | 378 ± 70 * (10) | 71.17 ± 5.91 (6) | 80.59 ± 2.47* (4) |
| | *ani-1 + ani-2* | 380 ± 51 * (5) | 70.71 ± 4.50 (7) | ND |

**B**

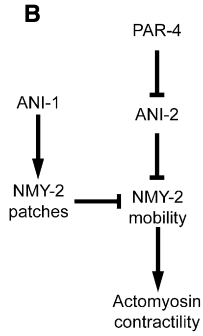


Figure 6. Depletion of *ani-1* Impairs Suppression of *par-4* Phenotypes by *ani-2(RNAi)*

(A) Quantifications of the duration of cytokinetic furrow ingression, distribution of PAR-6::GFP fluorescence intensity, and maximal NMY-2::GFP FRAP in control embryos or embryos depleted for ANI-1 and/or ANI-2. The numbers in parentheses indicate the number of embryos assayed. *$p < 0.05$ (Student's t test) significantly different from the same strain treated with control*(RNAi)*. ND denotes not determined.

(B) A new PAR-4/LKB1 pathway to regulate actomyosin contractility. In normal embryos, PAR-4 prevents ectopic ANI-2 accumulation, thereby allowing the actomyosin cytoskeleton assembled by ANI-1 to be dynamically restructured during polarization and cytokinesis. When PAR-4 is depleted, ANI-2 increases and blocks actomyosin dynamics, possibly by competing with ANI-1 for the binding of one or many regulators, and actomyosin is properly assembled but poorly dynamic. This pathway does not directly regulate the activation of the PAR-1 kinase by PAR-4, which leads to proper localization of cell fate determinants by regulating MEX-5/6 activity. See also Figure S5.

embryos (Figure 6A). These results indicate that the suppression of *par-4* phenotypes by ANI-2 depletion requires the presence of the canonical anillin ANI-1 and support a model in which the contractility defects observed in *par-4* mutants are due to the perturbation of ANI-1 function by ANI-2 (Figure 6B).

Surprisingly, in FRAP experiments, depleting ANI-1 phenocopied ANI-2 depletion and resulted in a restoration of myosin mobility at the cortex of *par-4* mutant embryos (Figure 6A). However, the actomyosin cortex is severely disorganized in *ani-1(RNAi)* embryos: NMY-2 fails to coalesce into robust patches [19]. ANI-1-depleted embryos have normal polarity and can complete cytokinesis ([19]; Figure 6A), indicating that ANI-1 does not regulate contractility per se, but rather regulates the organization of the actomyosin cortex. We conclude that the gain of ANI-2 function observed in *par-4* embryos only affects cortical myosin turnover in NMY-2 patches and that disrupting the formation of these patches abrogates the negative regulation by ANI-2. This is consistent with previous reports indicating that the degree of organization of the actomyosin network inversely correlates with the turnover of its components [28–30].

## Discussion

In the present study, we explored the role of PAR-4 in the regulation of actomyosin contractility during early *C. elegans* embryonic development. We found that *par-4* mutations reduce the efficiency of actomyosin contractility during two important developmental events in the zygote: establishment of polarity and cytokinesis. We further demonstrated that PAR-4 promotes the turnover of myosin at the cortex of polarizing embryos. Finally, we showed that depletion of ANI-2, one of the anillin homologs in *C. elegans*, suppresses the actomyosin defects displayed by *par-4* mutants and that the presence of the canonical anillin scaffold ANI-1 is essential to achieve this suppression. Our results support a model in which ANI-2 negatively regulates actomyosin contractility by competing with the actomyosin-organizing function of ANI-1 downstream of PAR-4 signaling (Figure 6B). We propose that PAR-4 regulates cell polarity and actomyosin contractility dynamics by inhibiting ANI-2 and ensuring the mobility of cortical myosin during the first steps of *C. elegans* embryonic development.

Our results support observations [22] that PAR-4, although symmetrically localized in the embryo, regulates the anterior-directed actomyosin contractile flow. Although cortical flows were not totally abolished in *par-4* embryos, their speed was reduced by 30% compared to wild-type. As a consequence, the localization of cortical NMY-2::GFP and PAR-6::GFP was not fully restricted to the anterior half of *par-4* embryos. This is consistent with the observation that PAR-6 is aberrantly present in the posterior of dividing *par-4* mutant embryos [31]. It was also reported that blebs form during the first cytokinesis of *par-4* embryos [8]. Our study indicates that this phenotype results directly from defects in actomyosin dynamics during contractile ring assembly and specification of the cleavage plane. We showed that the contractile ring assembles more slowly, is inaccurately positioned, and ingresses more slowly in *par-4* mutants than in wild-type embryos. These cytokinesis defects are consistent with observations that *Drosophila lkb1* null mutants have an increased incidence of polyploidy, which could result from failed cytokineses [32].

We showed that disruption of *ani-2* restores normal actomyosin contractility in *par-4* embryos at fully restrictive temperature but suppresses *par-4* lethality only at semirestrictive temperature. Thus, the actomyosin defects of *par-4* mutants cannot be the only cause of *par-4* lethality. Indeed, *par-4* embryos also display missegregation of cell fate determinants such as PIE-1 and P granules, loss of cell-cycle asynchrony between the AB and $P_1$ blastomeres, and loss of differentiation and specification of tissues [8]. Depleting *ani-2* does not suppress these phenotypes. This suggests that PAR-4 functions upstream of at least two pathways in the early embryo: one that regulates cell fate specification by segregating PIE-1 and P granules and that depends on PAR-1 and MEX-5 proteins [21, 33], and another promoting efficient actomyosin contractility through negative regulation of ANI-2. The defects observed in the two pathways might have additive effects on embryonic viability, which could explain the reversion of actomyosin phenotypes by *ani-2(RNAi)* treatment at high restrictive temperature while embryonic lethality remains. Consistent with this notion, loss of PAR-4 activity completely abrogates the proper segregation of cell fate determinants but does not result in a complete mislocalization of PAR-6. Restoring normal actomyosin might therefore only promote viability at

(I) Quantification of the percentage of maximal fluorescence recovery ± SEM for each condition. In all panels, scale bar is 10 μm, *$p < 0.05$ (Student's t test) compared to wild-type embryos treated with control*(RNAi)*, and **$p < 0.05$ (Student's t test) compared to *par-4* mutant embryos treated with control*(RNAi)*. See also Figure S4.

semipermissive temperatures, when more PAR-4 is active in the embryo and cell fate determinants are properly segregated. The antagonistic relationship between PAR-4 and ANI-2 may also regulate other actomyosin contractility processes, such as gastrulation and elongation, that are essential later in embryonic development.

How could a gain of ANI-2 function reduce actomyosin contractility in *par-4* mutants? Several lines of evidence support a role in negative regulation of actomyosin by this short *C. elegans* anillin isoform. First, ANI-2 is enriched on the rachis lining of the syncitial oogenic gonad, and its disruption leads to a precocious individualization of oocytes, a process that requires active myosin [19, 34]. Therefore, the diminution of ANI-2 in this context could allow abnormal myosin activation, thus driving oocyte cellularization. Second, sequence analysis of *C. elegans* anillin [19] indicates that ANI-2 lacks the N-terminal domain that allows binding to myosin and F-actin but possesses the C-terminal AHD and PH domains implicated in binding actomyosin regulators such as RhoA, MgcRacGAP, and septins [23–26]. This suggests a model in which ANI-2 uncouples myosin and F-actin from some of their major regulators in a dominant-negative fashion by competing with the function of the canonical anillin ANI-1. In support of this model, we find that *ani-2* inhibition can restore normal PAR-6 localization and cytokinetic ring ingression in *par-4* mutants only when ANI-1 is present (Figure 6A). However, the role of ANI-1 in this model is ambiguous, because depleting ANI-1 in *par-4* mutant embryos suppresses myosin turnover during polarization but enhances ingression defects during cytokinesis. We believe that this apparent discrepancy is due to the known function of ANI-1 in actomyosin organization and a differential requirement for actomyosin function during these two cellular processes. ANI-1 promotes actomyosin organization and assembly, which itself was reported to negatively regulate myosin turnover in other systems [28, 29, 35]. Therefore, a depletion of ANI-1 in the early embryo would result in increased myosin mobility due to a defect in myosin organization into patches. Why would this have a different impact on cytokinesis? During polarization, myosin turnover is critical to promote cytoplasmic flows [17], but flows can occur in *ani-1(RNAi)* embryos in which the cortex is disorganized [19], indicating that myosin turnover is the limiting process at this stage. However, formation of the contractile ring during cytokinesis requires a high degree of actomyosin organization [36] but does not depend heavily on myosin turnover [37, 38]. Because of its important function in promoting actomyosin organization, depleting ANI-1 would therefore differentially affect these two processes when "dominant-negative" ANI-2 is functional. Our results therefore indicate that the mechanism by which *par-4* affects actomyosin contractility relies on a finely tuned balance between the two anillin isoforms in the early *C. elegans* embryo. Given the conserved function of PAR-4 in regulating cell polarity, it will be interesting to investigate whether this LKB1-dependent pathway is conserved in other species and cell types.

## Experimental Procedures

All strains were maintained as described by Brenner [39] and were grown at 15°C and assayed at 25°C unless otherwise stated. For time-lapse imaging, embryos were mounted as previously described [1] and image analysis was performed using various quantification tools. For more information, please see the Supplemental Experimental Procedures.

## Supplemental Information

Supplemental Information includes five figures, one table, Supplemental Experimental Procedures, and three movies and can be found with this article online at doi:10.1016/j.cub.2011.01.010.

## Acknowledgments

We are grateful to Karen Oegema, the *C. elegans* Gene Knockout Consortium, and the *Caenorhabditis* Genetics Center for strains and reagents. We also thank Paul Maddox, Jonas Dorn, and members of the Maddox and Labbé laboratories for helpful discussions and comments on the manuscript, Sabrina Bergeron for technical assistance, and Christian Charbonneau of IRIC's Bio-Imaging Core Facility for technical help with image acquisition. N.T.C. was a research fellow of Fondation pour la Recherche Medicale (France) and presently holds a fellowship from les Fonds de Recherche en Santé du Québec (FRSQ). M.M. holds a fellowship from the Boehringer Ingelheim Foundation. A.S.M. is supported by a salary award from the FRSQ. This work was funded by a grant from the Canadian Institutes of Health Research (158715) to J.-C.L., who holds the Canada Research Chair in Cell Division and Differentiation. IRIC is supported in part by the Canadian Center of Excellence in Commercialization and Research, the Canada Foundation for Innovation, and the FRSQ.

Received: September 6, 2010
Revised: December 8, 2010
Accepted: January 5, 2011
Published online: January 27, 2011

## References

1. Sulston, J.E., Schierenberg, E., White, J.G., and Thomson, J.N. (1983). The embryonic cell lineage of the nematode *Caenorhabditis elegans*. Dev. Biol. *100*, 64–119.
2. Kemphues, K.J., Priess, J.R., Morton, D.G., and Cheng, N.S. (1988). Identification of genes required for cytoplasmic localization in early *C. elegans* embryos. Cell *52*, 311–320.
3. Hyenne, V., Chartier, N.T., and Labbé, J.C. (2010). Understanding the role of asymmetric cell division in cancer using *C. elegans*. Dev. Dyn. *239*, 1378–1387.
4. Goldstein, B., and Hird, S.N. (1996). Specification of the anteroposterior axis in *Caenorhabditis elegans*. Development *122*, 1467–1474.
5. Hird, S.N., and White, J.G. (1993). Cortical and cytoplasmic flow polarity in early embryonic cells of *Caenorhabditis elegans*. J. Cell Biol. *121*, 1343–1355.
6. Munro, E., Nance, J., and Priess, J.R. (2004). Cortical flows powered by asymmetrical contraction transport PAR proteins to establish and maintain anterior-posterior polarity in the early *C. elegans* embryo. Dev. Cell *7*, 413–424.
7. Watts, J.L., Morton, D.G., Bestman, J., and Kemphues, K.J. (2000). The *C. elegans par-4* gene encodes a putative serine-threonine kinase required for establishing embryonic asymmetry. Development *127*, 1467–1475.
8. Morton, D.G., Roos, J.M., and Kemphues, K.J. (1992). *par-4*, a gene required for cytoplasmic localization and determination of specific cell types in *Caenorhabditis elegans* embryogenesis. Genetics *130*, 771–790.
9. Giardiello, F.M., Brensinger, J.D., Tersmette, A.C., Goodman, S.N., Petersen, G.M., Booker, S.V., Cruz-Correa, M., and Offerhaus, J.A. (2000). Very high risk of cancer in familial Peutz-Jeghers syndrome. Gastroenterology *119*, 1447–1453.
10. Sanchez-Cespedes, M. (2007). A role for *LKB1* gene in human cancer beyond the Peutz-Jeghers syndrome. Oncogene *26*, 7825–7832.
11. Jansen, M., Ten Klooster, J.P., Offerhaus, G.J., and Clevers, H. (2009). LKB1 and AMPK family signaling: The intimate link between cell polarity and energy metabolism. Physiol. Rev. *89*, 777–798.
12. Alessi, D.R., Sakamoto, K., and Bayascas, J.R. (2006). LKB1-dependent signaling pathways. Annu. Rev. Biochem. *75*, 137–163.
13. Hawley, S.A., Boudeau, J., Reid, J.L., Mustard, K.J., Udd, L., Mäkelä, T.P., Alessi, D.R., and Hardie, D.G. (2003). Complexes between the LKB1 tumor suppressor, STRAD alpha/beta and MO25 alpha/beta are upstream kinases in the AMP-activated protein kinase cascade. J. Biol. *2*, 28.

14. Woods, A., Johnstone, S.R., Dickerson, K., Leiper, F.C., Fryer, L.G., Neumann, D., Schlattner, U., Wallimann, T., Carlson, M., and Carling, D. (2003). LKB1 is the upstream kinase in the AMP-activated protein kinase cascade. Curr. Biol. *13*, 2004–2008.
15. Baas, A.F., Kuipers, J., van der Wel, N.N., Batlle, E., Koerten, H.K., Peters, P.J., and Clevers, H.C. (2004). Complete polarization of single intestinal epithelial cells upon activation of LKB1 by STRAD. Cell *116*, 457–466.
16. ten Klooster, J.P., Jansen, M., Yuan, J., Oorschot, V., Begthel, H., Di Giacomo, V., Colland, F., de Koning, J., Maurice, M.M., Hornbeck, P., and Clevers, H. (2009). Mst4 and Ezrin induce brush borders downstream of the Lkb1/Strad/Mo25 polarization complex. Dev. Cell *16*, 551–562.
17. Mayer, M., Depken, M., Bois, J.S., Jülicher, F., and Grill, S.W. (2010). Anisotropies in cortical tension reveal the physical basis of polarizing cortical flows. Nature *467*, 617–621.
18. Piekny, A.J., and Maddox, A.S. (2010). The myriad roles of Anillin during cytokinesis. Semin. Cell Dev. Biol. *21*, 881–891.
19. Maddox, A.S., Habermann, B., Desai, A., and Oegema, K. (2005). Distinct roles for two *C. elegans* anillins in the gonad and early embryo. Development *132*, 2837–2848.
20. Lizcano, J.M., Göransson, O., Toth, R., Deak, M., Morrice, N.A., Boudeau, J., Hawley, S.A., Udd, L., Mäkelä, T.P., Hardie, D.G., and Alessi, D.R. (2004). LKB1 is a master kinase that activates 13 kinases of the AMPK subfamily, including MARK/PAR-1. EMBO J. *23*, 833–843.
21. Narbonne, P., Hyenne, V., Li, S., Labbé, J.C., and Roy, R. (2010). Differential requirements for STRAD in LKB1-dependent functions in *C. elegans*. Development *137*, 661–670.
22. Cheeks, R.J., Canman, J.C., Gabriel, W.N., Meyer, N., Strome, S., and Goldstein, B. (2004). *C. elegans* PAR proteins function by mobilizing and stabilizing asymmetrically localized protein complexes. Curr. Biol. *14*, 851–862.
23. D'Avino, P.P., Takeda, T., Capalbo, L., Zhang, W., Lilley, K.S., Laue, E.D., and Glover, D.M. (2008). Interaction between Anillin and RacGAP50C connects the actomyosin contractile ring with spindle microtubules at the cell division site. J. Cell Sci. *121*, 1151–1158.
24. Gregory, S.L., Ebrahimi, S., Milverton, J., Jones, W.M., Bejsovec, A., and Saint, R. (2008). Cell division requires a direct link between microtubule-bound RacGAP and Anillin in the contractile ring. Curr. Biol. *18*, 25–29.
25. Kinoshita, M., Field, C.M., Coughlin, M.L., Straight, A.F., and Mitchison, T.J. (2002). Self- and actin-templated assembly of mammalian septins. Dev. Cell *3*, 791–802.
26. Piekny, A.J., and Glotzer, M. (2008). Anillin is a scaffold protein that links RhoA, actin, and myosin during cytokinesis. Curr. Biol. *18*, 30–36.
27. Maddox, A.S., Lewellyn, L., Desai, A., and Oegema, K. (2007). Anillin and the septins promote asymmetric ingression of the cytokinetic furrow. Dev. Cell *12*, 827–835.
28. Lister, I.M., Tolliday, N.J., and Li, R. (2006). Characterization of the minimum domain required for targeting budding yeast myosin II to the site of cell division. BMC Biol. *4*, 19.
29. Yumura, S., Yoshida, M., Betapudi, V., Licate, L.S., Iwadate, Y., Nagasaki, A., Uyeda, T.Q., and Egelhoff, T.T. (2005). Multiple myosin II heavy chain kinases: Roles in filament assembly control and proper cytokinesis in Dictyostelium. Mol. Biol. Cell *16*, 4256–4266.
30. Murthy, K., and Wadsworth, P. (2005). Myosin-II-dependent localization and dynamics of F-actin during cytokinesis. Curr. Biol. *15*, 724–731.
31. Hung, T.J., and Kemphues, K.J. (1999). PAR-6 is a conserved PDZ domain-containing protein that colocalizes with PAR-3 in *Caenorhabditis elegans* embryos. Development *126*, 127–135.
32. Lee, J.H., Koh, H., Kim, M., Kim, Y., Lee, S.Y., Karess, R.E., Lee, S.H., Shong, M., Kim, J.M., Kim, J., and Chung, J. (2007). Energy-dependent regulation of cell structure by AMP-activated protein kinase. Nature *447*, 1017–1020.
33. Tenlen, J.R., Molk, J.N., London, N., Page, B.D., and Priess, J.R. (2008). MEX-5 asymmetry in one-cell *C. elegans* embryos requires PAR-4- and PAR-1-dependent phosphorylation. Development *135*, 3665–3675.
34. Wolke, U., Jezuit, E.A., and Priess, J.R. (2007). Actin-dependent cytoplasmic streaming in *C. elegans* oogenesis. Development *134*, 2227–2236.
35. Ray, R.M., Guo, H., Patel, M., Jin, S., Bhattacharya, S., and Johnson, L.R. (2007). Role of myosin regulatory light chain and Rac1 in the migration of polyamine-depleted intestinal epithelial cells. Am. J. Physiol. Gastrointest. Liver Physiol. *292*, G983–G995.
36. Dorn, J.F., Zhang, L., Paradis, V., Edoh-Bedi, D., Jusu, S., Maddox, P.S., and Maddox, A.S. (2010). Actomyosin tube formation in polar body cytokinesis requires Anillin in *C. elegans*. Curr. Biol. *20*, 2046–2051.
37. Carvalho, A., Desai, A., and Oegema, K. (2009). Structural memory in the contractile ring makes the duration of cytokinesis independent of cell size. Cell *137*, 926–937.
38. Zhou, M., and Wang, Y.L. (2008). Distinct pathways for the early recruitment of myosin II and actin to the cytokinetic furrow. Mol. Biol. Cell *19*, 318–326.
39. Brenner, S. (1974). The genetics of *Caenorhabditis elegans*. Genetics *77*, 71–94.